Rare Metal Materials and Engineering
Volume 49, Issue 6, June 2020
Available online at www.rmme.ac.cn

Science Press

Cite this article as: Rare Metal Materials and Engineering, 2020, 49(6): 1854-1859.

ARTICLE

Effect of Crystallographic Orientation on Nano-indentation Behavior of Nickel Based Single Crystal Super Alloys

Yan Wuzhu, Li Youliang, Wen Zhixun, Zou Shaohua, Duan Zuhang

Northwestern Polytechnical University, Xi'an 710129, China

Abstract: In order to investigate the effect of crystallographic orientation on the nano-indentation behaviors of single crystal super alloys, the nano-indentation experiments were carried out using a Berkovich indenter with an atomic force microscope. The specimens are nickel based single crystal super alloys with crystallographic orientations of [001], [011] and [111]. Experimental results show that the indentation load-depth curve, hardness and elastic modulus are remarkably influenced by crystallographic orientation. It is found that the shape and volume fraction of γ' strengthening phase are dependent on crystallographic orientation, which will influence the mechanical properties. The nano-indentation experiments performed on three typical crystallographic orientations are simulated by crystal plasticity theory to investigate the indentation responses and the resolved shear stress, and the simulation results show a good agreement with the experiment results.

Key words: nano-indentation; single crystal super alloys; crystallographic orientation; crystal plasticity theory

The nickel based single crystal super alloys have been widely applied on thermal parts of aircraft engine due to their excellent mechanical performance at high temperatures. Compared to polycrystalline alloys, the single crystal super alloys have no grain boundaries, so the boundary weakening and grain boundary cracking are avoided. However, the mechanical properties of nickel based single crystal super alloys exhibit strong anisotropy. It is reported that the percentage elongation and life of nickel based single crystal super alloys are strongly influenced by the crystallographic orientation[1].

Most researches on the mechanical properties of single crystal super alloys are based on conventional uniaxial tensile/compressive tests which have strict requirements on specimen geometry and griping fixtures. Moreover, the conventional tests can not reflect the local mechanical properties of indented materials. On the contrary, the indentation test has attracted much attention due to its simple, fast and effective merits. In the indentation test, only a small quantity of materials are needed, which allows specimen geometry simpler and avoids the need of griping of specimen threads.

Compared to conventional uniaxial tensile/compressive test, the nano-indentation test can help to understand the deformation details of anisotropic single crystal super alloys. Zambaldi et al[2] presented the crystal-plasticity deformation of a single-crystal nickel-base super alloy at room temperature and the microstructure development during subsequent recrystallization. Sabnis[3] discussed crystal plasticity simulation and conducted experiments of cylindrical indentation on nickel base single crystal superalloy specimens. The finite element (FE) prediction was compared to the detailed experimental observation of slip lines on the free lateral surface of the substrate. Hu[4] simulated nano-indentation with diamond indenter on pure Ni and the γ/γ'-phase in a Ni-base single-crystal super alloy by molecular dynamics method. Li[5] investigated the anisotropic micromechanical properties of single-crystal nickel-based super alloy DD9 with four crystallographic orientations including (001), (215), (405) and (605) by micro-indentation test, employing a sharp Berkovich indenter. Recently, Yan[6] performed impression creep on

Received date: September 11, 2019
Foundation item: National Natural Science Foundation of China (51905432); Natural Science Basic Research Program of Shaanxi (2018JQ1030); the Fundamental Research Funds for the Central Universities (310201906zy002)
Corresponding author: Yan Wuzhu, Ph. D., Associate Professor, School of Mechanics, Civil Engineering and Architecture, Northwestern Polytechnical University, Xi'an 710129, P. R. China, Tel: 0086-29-88431000, E-mail: yanwuzhu@nwpu.edu.cn

single crystal super alloys and found that the impression creep response and stress distribution are dependent on the crystallographic orientation. Most previous researches have focused on the micro/meso mechanism of indentation deformation. However, the effects of crystallographic orientation on the elastic modulus, hardness as well as the anisotropic indentation response have seldom been fully understood.

The present work aims to address the aforementioned gap by performing indentation tests on nickel based single crystal super alloys using a Berkovich indenter. The influences of crystallographic orientation on load-depth curve, hardness, elastic modulus and resolved stress distribution were revealed. The experiment results were rationalized by crystal plasticity finite element analysis of indentation tests.

1 Experiment

The material used in this work was nickel based single crystal super alloy DD6 with standard heat treatment process: 1290 °C, 1 h+1300 °C, 2 h+1315 °C, 4 h, air cooling+1120 °C, 4 h, air cooling+870 °C, 32 h, air cooling. The crystallographic orientations of the specimens were selected as [001], [011] and [111].

The specimens used in this work were rectangular with the size of 5 mm×5 mm×3 mm. The indented surface was polished. The Hysitron TI950 nano-indentation equipment shown in Fig.1 was employed to carry out the nano-indentation experiment. The loading history of the nano-indentation experiment is shown in Fig.2, with the maximum loads of 5 and 10 mN for each crystallographic orientation.

2 Numerical Simulation

2.1 Crystal plasticity theory

The constitutive equations of crystal plasticity theory presented here were firstly developed by Taylor[7] and Hill[8] et al. The plastic deformation was realized by crystal dislocation slip and the deformation by diffusion.

For the crystal plasticity model, the total deformation gradient $\boldsymbol{F}$ consists of elastic and plastic components:

$$\boldsymbol{F} = \boldsymbol{F}^{\mathrm{e}} \cdot \boldsymbol{F}^{\mathrm{p}} \tag{1}$$

Lattice vectors stretch and rotate as the crystal deforms and rotates. The slip system α and the slip directions $\boldsymbol{m}^{(\alpha)}$ can be written as:

$$\boldsymbol{m}^{*(\alpha)} = \boldsymbol{F}^{\mathrm{e}}\boldsymbol{m}^{(\alpha)} \tag{2}$$

The normal vector of the slip plane can be written as:

$$\boldsymbol{n}^{*(\alpha)} = [(\boldsymbol{F}^{\mathrm{e}})^{-1}]^{\mathrm{T}}\boldsymbol{n}^{(\alpha)} \tag{3}$$

The current velocity gradient can be expressed as:

$$\boldsymbol{L} = \dot{\boldsymbol{F}}\boldsymbol{F}^{-1} = \boldsymbol{L}^{\mathrm{e}} + \boldsymbol{L}^{\mathrm{F}} \tag{4}$$

where $\boldsymbol{L}$ can also be written as:

$$\boldsymbol{L} = \boldsymbol{D} + \boldsymbol{W} \tag{5}$$

where $\boldsymbol{W}$ and $\boldsymbol{D}$ are the symmetric rates of the spin and stretching tensors, respectively. Since plastic deformation is resulted from dislocation slip, the plastic velocity gradient can be written as a linear function of the shear rates:

$$\boldsymbol{L}^{P} = \sum_{\alpha=1}^{N} \boldsymbol{P}^{(\alpha)}\dot{\gamma}^{(\alpha)} \tag{6}$$

where $\dot{\gamma}^{(\alpha)}$ is the rate of slipping, $\boldsymbol{P}^{(\alpha)}$ is the Schmid tensor that can be expressed as:

$$\boldsymbol{P}^{(\alpha)} = \frac{\boldsymbol{1}}{\boldsymbol{2}}(\boldsymbol{m}^{*(\alpha)} \otimes \boldsymbol{n}^{*(\alpha)} + \boldsymbol{n}^{*(\alpha)} \otimes \boldsymbol{m}^{*(\alpha)}) \tag{7}$$

Defining $\boldsymbol{\sigma}$ and $\boldsymbol{\tau}$ as the Cauchy stress tensor and the weighted Cauchy stress tensor, we have:

$$\boldsymbol{\tau} = (\det\boldsymbol{F})\boldsymbol{\sigma} \tag{8}$$

and

$$\boldsymbol{T} = \boldsymbol{F}^{\mathrm{e}}\boldsymbol{\tau}(\boldsymbol{F}^{\mathrm{e}})^{-1} \tag{9}$$

The second Piola-Kirchhoff stress tensor is relative to the intermediate configuration.

The resolved shear stress is the component of the traction along the direction of slip through the Schmid tensor as follows:

$$\boldsymbol{\tau}^{(\alpha)} = \boldsymbol{P}^{(\alpha)} : \boldsymbol{T} \tag{10}$$

where $\boldsymbol{P}^{(\alpha)}$ is Schmid factor of slip system α.

For the rate-dependent constitutive formulation here, the slip rate is a function of resolved shear stresses and reference stresses. The shearing rate was given by Peirce[9]:

$$\dot{\gamma}^{(\alpha)} = \dot{\gamma}_0^{(\alpha)}[\frac{\tau^{(\alpha)}}{g^{(\alpha)}}][\left|\frac{\tau^{(\alpha)}}{g^{(\alpha)}}\right|]^{\frac{1}{m}-1} \tag{11}$$

where $g^{(\alpha)}$ is the resistance to shear of the slip system, $\dot{\gamma}_0^{(\alpha)}$ is

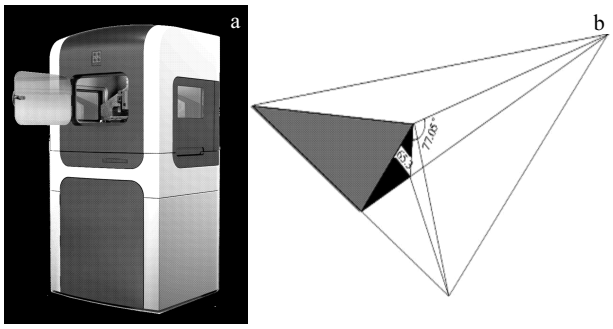

Fig.1 TI950 nano-indentation equipment (a) and Berkovich indenter (b)

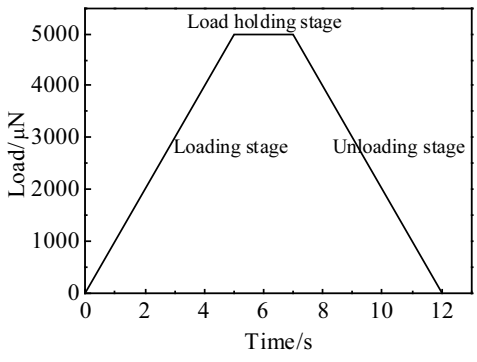

Fig.2 Loading history of nano-indentation tests with the maximum loads of 5 mN

the reference shear rate, m is the strain rate sensitivity exponent. The function $g^{(\alpha)}$ is the current strain hardening state. Here, we assume that $g^{(\alpha)}$ is dependent on slip strain:

$$g^{(\alpha)} = g^{(\alpha)}(\gamma) \tag{12}$$

where

$$\gamma = \sum_{\alpha} \left| \gamma^{(\alpha)} \right| \tag{13}$$

It is assumed that the strain hardening can be specified by the evolution of $g^{(\alpha)}$, which can be expressed as follows[8]:

$$\dot{g}^{(\alpha)} = \sum\nolimits_{\beta} h_{\alpha\beta} \left| \dot{\gamma}^{(\beta)} \right| \tag{14}$$

where $h_{\alpha\beta}$ is a function of γ.

$$h_{\alpha\beta} = q_{\alpha\beta} h_{\beta} \quad \text{(no sum on } \beta\text{)} \tag{15}$$

where h_{β} is the single hardening rate, $q_{\alpha\beta}$ is the latent hardening matrix. Here we choose[10]:

$$h_{\beta} = h_0 (1 - \frac{g^{(\beta)}}{\tau_s})^{\alpha} \tag{16}$$

where τ_s, h_0 and β are hardening parameters, which are the same for all slip systems.

2.2 Finite element model

Three dimensional models of nano-indentations performed on single crystals were developed, as shown in Fig.3. The geometry sizes of specimen and indenter were the same as the actual ones. The indenter made of diamond was modeled as rigid, while the specimen was modeled as a 3D deformable solid. In order to reduce computing cost, the mesh was refined as approaching to the indented area. The element types of the specimen and the indenter were C3D8R and R3D4, respectively.

The normal contact condition between the indenter and specimen was hard contact, while the tangential contact condition was finite sliding with no friction. The components of nickel based single crystal super alloy were modeled by crystal plasticity theory introduced in Section 3.1. The components were incorporated into finite element simulations via a specially written UMAT in ABAQUS, and its effectiveness has been validated by other independent studies[6].

3 Results and Discussion

3.1 Load-depth curve

Fig.4 shows the load-depth curves of three different

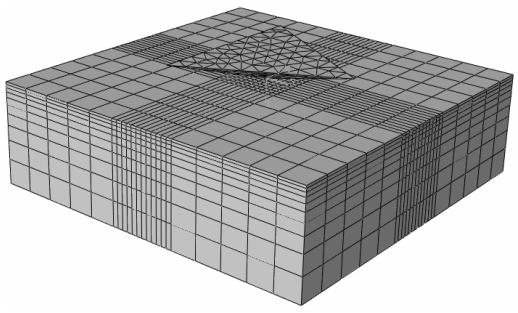

Fig.3 Three dimensional finite element model of nano-indentation

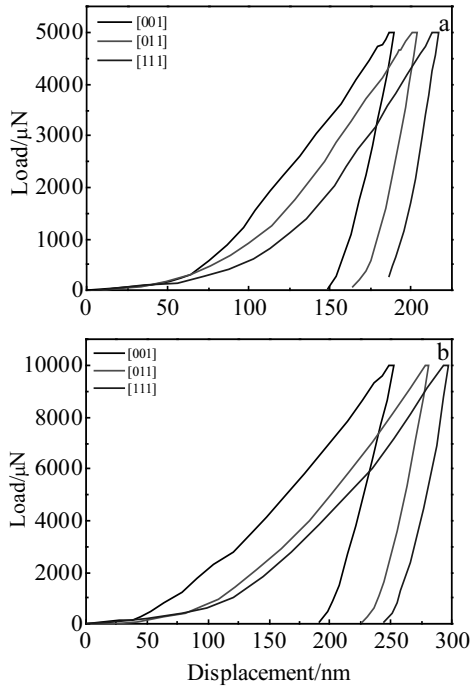

Fig.4 Effect of crystallographic orientation on load-depth curves with the maximum load of 5 mN (a) and 10 mN (b)

oriented specimens. The maximum loads are 5 (Fig.4a) and 10 mN (Fig.4b). It can be seen that the linear elastic stage is very short. The influence of crystallographic orientation on the maximum indentation depth is remarkable. The maximum indentation depth is resulted from [111]-orientation while the smallest one is resulted from [001]-orientation. This is because the mechanical properties of single crystal super alloys exhibit strong anisotropy.

Fig.5 shows the elastic recovery rates resulting from [001]-, [011]- and [111]-orientations. It can be seen that the [001]-orientation brings the largest elastic recovery rate while the [111]-orientation brings the smallest one, indicating that [111]-orientation shows the largest plastic deformation while the [001]-orientation has the smallest one. The plastic deformation of nickel based single crystal super alloy is mainly realized by crystallographic slipping. There are 3 groups of slip system families including octahedron slip system family (Oct1, {111}<110> slip system), hexahedron slip system family (Cub, {100}<110> slip system) and dodecahedron slip system family (Oct2, {111} <112> slip system). In the case of compression, the activation of slip systems is dependent on crystallographic orientation. For [001]- and [011]-orientations, octahedron slip system family is activated. For [111]-orientation, the hexahedron slip system family is activated as the main slip system accompanied by a few other slip systems, resulting in multi-system slip. Although both of [001]- and [011]-orientations activate {111}<110> system, the [011]-orientation activates two groups of {111}<110> slip

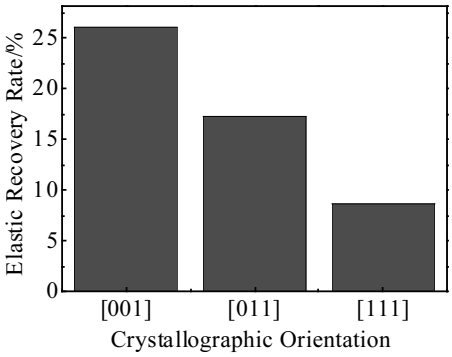

Fig.5 Elastic recovery rates resulting from [001]-, [011]- and [111]-orientations

systems simultaneously, while the [001]-orientation activates only one single octahedron slip system. Hence, the [111]-orientation is the orientation easiest to slipping for dislocation, exhibiting the best plasticity deformation capability under compression.

From the nano-indentation experiment results, it can be inferred that the [111]-orientation activates most slip systems, resulting in the smallest slip resistance, while the [001]-orientation activates the least slip systems, resulting in the largest slip resistance.

3.2 Elastic modulus and hardness

The elastic modulus can be derived from the load-depth curve by Oliver and Pharr's equation [11]:

$$E^* = \beta \frac{\sqrt{\pi}}{2} \frac{S}{\sqrt{A_c}} \quad (17)$$

where S is the unloading stiffness, A_c is the projected contact area, β is the shape factor, with β=1 for axisymmetric indenter and β=1.03~1.05 for indenters with square or rectangular cross-sections.

The derived elastic modulus and hardness are plotted as a function of crystallographic orientation, as shown in Fig.6. It can be seen that the [111]-orientation exhibits the largest elastic modulus, while the [001]-orientation exhibits the smallest one. For hardness, however, the crystallographic orientation shows the opposite influence. This is mainly because the arrangement and density of atoms for different crystallographic planes are varied. The distance between neighboring atoms is the largest on {111} crystallographic plane. However, for fcc metals, the {111} crystallographic plane has the largest atom density, resulting in the strongest bonding interaction and the largest elastic modulus. The opposite results can be obtained for {100} crystallographic plane.

3.3 Effect of creep time and microstructures

Nickel based single crystal super alloys generally work at high temperatures. Hence, creep plays an important role in the evolution of microstructures. The elastic modulus of strengthening phase γ' and matrix phase γ at different creep time is

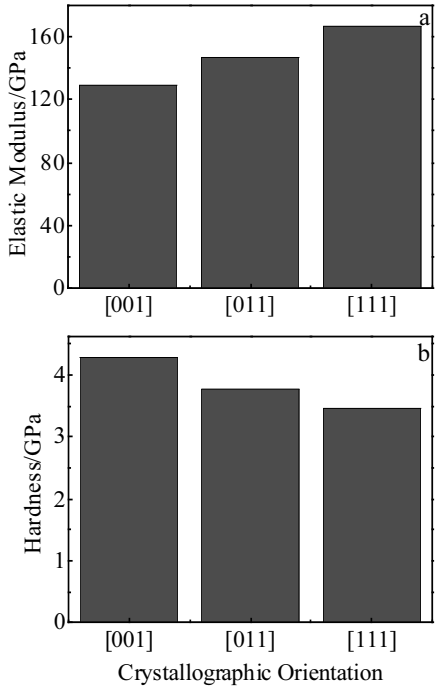

Fig.6 Elastic modulus (a) and hardness (b) of [001], [011] and [111] orientations

derived from load-depth curves. From Fig.7, it can be seen that elastic modulus of strengthening phase γ' is larger than that of matrix phase γ at the same creep time. However, the strengthening phase γ' is more sensitive to creep time than matrix phase γ. In other words, a larger increase of elastic modulus can be obtained by the strengthening phase γ' at the same creep time.

3.4 Stress distribution

In order to validate the developed FE model, the load-depth curves resulting from FE simulations are compared with those obtained from experiment counterparts, as shown in Fig.8. It can be seen that the load-depth curves resulting from FE simulations agree well with experimental results. It proves that the adoption of crystal plasticity theory in the FE simulation is

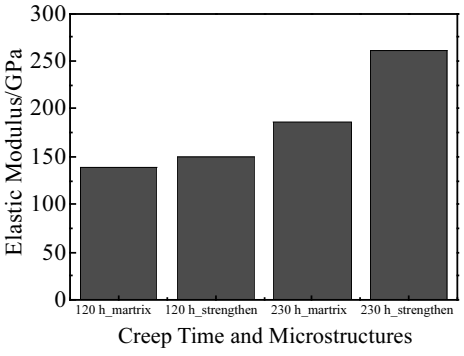

Fig.7 Effect of creep time and microstructures on elastic modulus

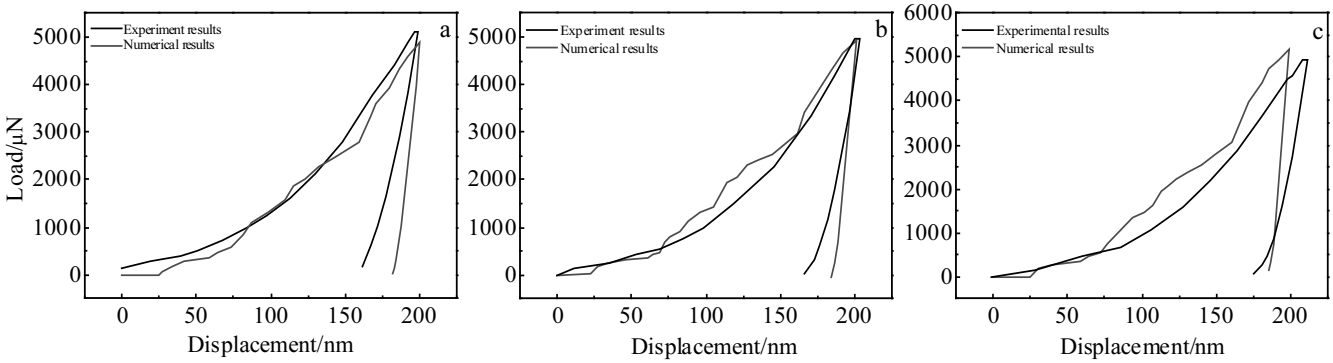

Fig.8 Load-depth curves obtained from experiments and FE simulation: (a) [001], (b) [011], and (c) [111]

acceptable. The distribution of resolved shear stress at the maximum depth is shown in Fig.9. It can be seen that the distribution of resolved stress is remarkably influenced by crystallographic orientation. The distribution of resolved shear stress exhibits fourfold, twofold and threefold symmetry in shape for [001]-, [011]- and [111]-orientations, respectively, which agrees well with Xu's results[12]. The largest resolved shear stress is brought by [111]-orientation, while the smallest one is brought by [011]-orientation. The distribution of resolved shear stress in vertical direction is also dependent on crystallographic orientation. The thickness of resolved shear stress resulting from [001]-orientation is smaller than that resulting from other two directions. For [111]-orientation, the resolve shear stress is mainly distributed in the vertical direction which is coaxial with the indenter. For [001]- and [011]-orientations, however, the resolved shear stress is distributed in two directions, and the largest intersection angle of the two directions is brought by [001]-orientation.

3.5 Crystallographic microstructure and morphology

Prior to indentation test, the specimens are polished and etched. The microstructures of nickel based single crystal super alloys with different orientations were then observed by SEM (Fig.10). The microstructure of DD6 is mainly composed by γ' strengthening phase and γ matrix phase, and remarkably influenced by crystallographic orientation. The γ' strengthening phase of [001]-orientation is square in shape, and vertical to the matrix interchannel. The matrix interchannel of [011]-orientation is slant, and the γ' strengthening phase is not a regular square in shape. For [111]-orientation, the slant angle of the matrix interchannel is

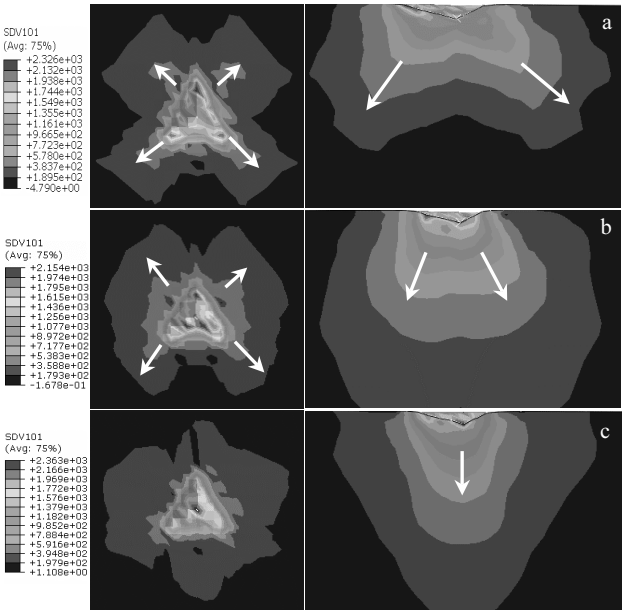

Fig.9 Distribution of the maximum resolved shear stress at the maximum depth: (a) [001], (b) [011], and (c) [111]

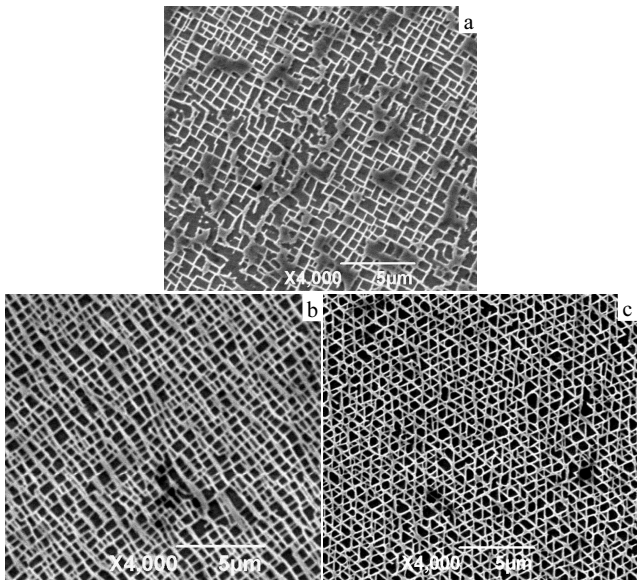

Fig.10 SEM images of nickel based single crystal super alloys with different orientations: (a) [001], (b) [011], and (c) [111]

further increased, and the γ' strengthening phase is triangle in shape. The largest and smallest volume fractions of γ' strengthening phase are resulted from [111]- and [001]-orientations, respectively. For nickel based single crystal super alloys, the stiffness of γ' strengthening phase is much larger than that of matrix. The anisotropic strength is mainly determined by the shape and volume fraction of γ' strengthening phase which is the main obstacle to dislocation. This explains why the largest and smallest strengths are brought by [111]- and [001]-orientations, respectively.

4 Conclusions

1) Metallographic phase microstructure observation of specimens shows that [111]-orientation has the highest volume fraction of strengthening phase γ' while the [001]-orientation has the smallest one. The strengthening phases are triangle and square in shape for [111]- and [001]-orientations, respectively. The elastic modulus derived from nano-indentation tests obeys the sequence of $E_{i\text{-}[111]}>E_{i\text{-}[011]}>E_{i\text{-}[001]}$, while the hardness shows the contrary results: $H_{i\text{-}[001]}> H_{i\text{-}[011]}> H_{i\text{-}[111]}$.

2) The elastic recovery rates of single crystals with different orientations are affected by the crystallographic orientation. The largest and smallest elastic recovery rates are resulted from the [001]- and [111]-orientations, respectively, suggesting that the [111]-orientation has the best plastic deformation capability.

3) The load-depth curves obtained from FE simulation agree well with those obtained from experiments, which validates the crystal plasticity theory. [111]- and [001]-orientations exhibit the largest and smallest resolved shear stresses, respectively, which implies that more slip systems are activated in [111]-orientation.

References

1 Yan W Z, Wen S F, Liu J *et al*. *Materials Science and Engineering A*[J], 2010, 527: 1850

2 Zambaldi C, Roters F, Raabe D *et al*. *Materials Science and Engineering A*[J], 2007, 454-455: 433

3 Sabnis P A, Forest S, Arakere N K *et al*. *International Journal of Plasticity*[J], 2013, 51: 200

4 Hu X J, Zheng B L, Hu T Y *et al*. *Acta Physica Sinica*[J], 2014, 63(17): 176

5 Li J H, Li F G, Dong J Z *et al*. *Journal of Nanomaterials*[J], 2015(9): 1

6 Yan W Z, Yuan X, Zhao W J *et al*. *Materials Science and Engineering A*[J], 2017, 707: 12

7 Taylor G I. *Journal of the Japan Institute of Metals*[J], 1938, 62: 307

8 Hill R, Rice J R. *Journal of the Mechanics and Physics of Solids*[J], 1972, 20: 401

9 Peirce D, Asaro R J, Needleman A. *Acta Metallurgica*[J], 1982, 30: 1087

10 Anand L, Kothari M. *Journal of the Mechanics and Physics of Solids*[J], 1996, 44(4): 525

11 Oliver W C, Pharr G M. *Journal of Materials Research*[J], 1992, 7: 1564

12 Xu B X, Yonezu A, Yue Z F *et al*. *Computer Materials Science*[J], 2009, 46: 275

晶体取向对镍基单晶高温合金纳米压痕行为的影响

闫五柱，李有亮，温志勋，邹绍华，段祖航

(西北工业大学，陕西 西安 710129)

摘 要：为了研究晶体取向对镍基单晶高温合金纳米压痕行为的影响，采用带原子力显微镜的 Berkovich 压头对[001], [011]和[111]取向的镍基单晶高温合金开展了纳米压痕试验。试验结果显示：晶体取向对压痕载荷-深度曲线、硬度和弹性模量有显著影响。晶体取向会影响 γ′强化相的形状和体积分数，进而会影响其力学性能。采用晶体塑性理论对 3 种典型晶体取向下的纳米压痕响应和分解切应力分布开展有限元模拟，模拟结果与试验结果符合得较好。

关键词：纳米压痕；单晶高温合金；晶体取向；晶体塑性理论

作者简介：闫五柱，男，1985 年生，博士，副教授，西北工业大学力学与土木建筑学院工程力学系，陕西 西安 710129，电话：029-88431000，E-mail: yanwuzhu@nwpu.edu.cn